# Genetic lineage tracing reveals poor angiogenic potential of cardiac endothelial cells

Tea Kocijan ⓘ [1], Michael Rehman[1], Andrea Colliva[1], Elena Groppa[1], Matteo Leban[1], Simone Vodret[1], Nina Volf ⓘ [1], Gabriele Zucca ⓘ [1], Ambra Cappelletto ⓘ [1], Giulia Maria Piperno[2], Lorena Zentilin ⓘ [3], Mauro Giacca ⓘ [3,4,5], Federica Benvenuti[2], Bin Zhou ⓘ [6], Ralf H. Adams ⓘ [7], and Serena Zacchigna ⓘ [1,4]*

[1]Cardiovascular Biology Laboratory, International Centre for Genetic Engineering and Biotechnology (ICGEB), Padriciano, 99, 34149 Trieste, Italy; [2]Cellular Immunology Laboratory, International Centre for Genetic Engineering and Biotechnology (ICGEB), 34149 Trieste, Italy; [3]Molecular Medicine Laboratory, International Centre for Genetic Engineering and Biotechnology (ICGEB), 34149 Trieste, Italy; [4]Department of Medical, Surgical and Health Sciences, University of Trieste, 34127 Trieste, Italy; [5]King's College London, British Heart Foundation Centre of Research Excellence, School of Cardiovascular Medicine & Sciences, London UK; [6]The State Key Laboratory of Cell Biology, CAS Center for Excellence on Molecular Cell Science, Shanghai Institute of Biochemistry and Cell Biology, Chinese Academy of Sciences, University of Chinese Academy of Sciences, Shanghai, China; and [7]Department of Tissue Morphogenesis, Max Planck Institute for Molecular Biomedicine, D-48149 Muenster, Germany

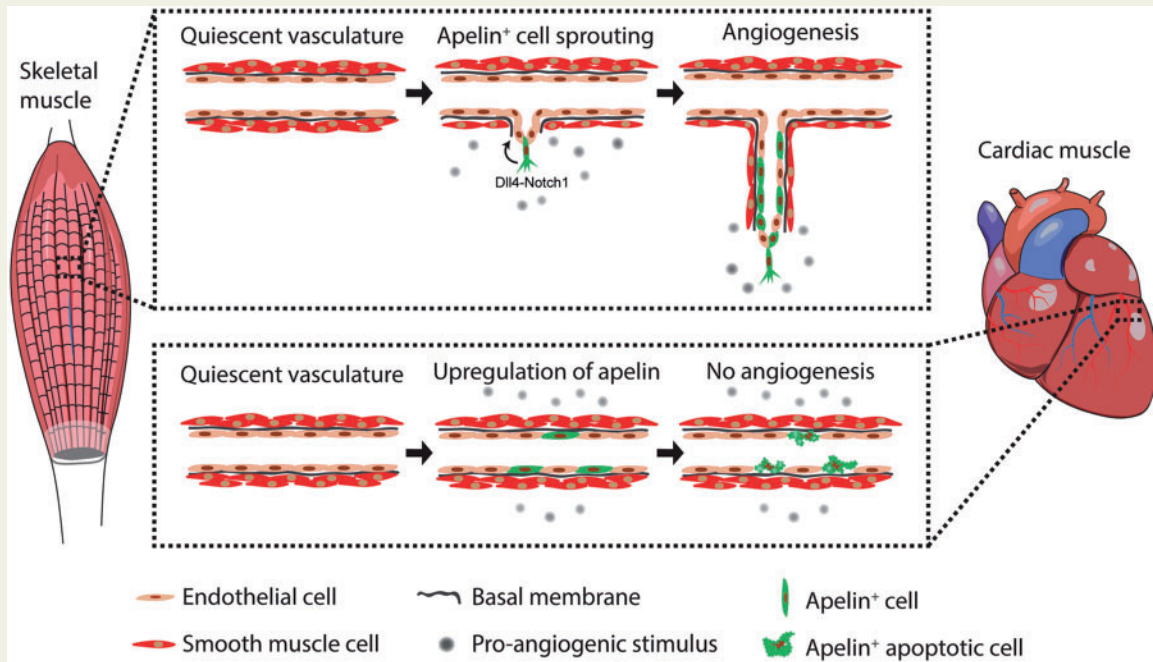| | |
|---|---|
| **Aims** | Cardiac ischaemia does not elicit an efficient angiogenic response. Indeed, lack of surgical revascularization upon myocardial infarction results in cardiomyocyte death, scarring, and loss of contractile function. Clinical trials aimed at inducing therapeutic revascularization through the delivery of pro-angiogenic molecules after cardiac ischaemia have invariably failed, suggesting that endothelial cells in the heart cannot mount an efficient angiogenic response. To understand why the heart is a poorly angiogenic environment, here we compare the angiogenic response of the cardiac and skeletal muscle using a lineage tracing approach to genetically label sprouting endothelial cells. |
| **Methods and results** | We observed that overexpression of the vascular endothelial growth factor in the skeletal muscle potently stimulated angiogenesis, resulting in the formation of a massive number of new capillaries and arterioles. In contrast, response to the same dose of the same factor in the heart was blunted and consisted in a modest increase in the number of new arterioles. By using Apelin-CreER mice to genetically label sprouting endothelial cells we observed that different pro-angiogenic stimuli activated Apelin expression in both muscle types to a similar extent, however, only in the skeletal muscle, these cells were able to sprout, form elongated vascular tubes activating Notch signalling, and became incorporated into arteries. In the heart, Apelin-positive cells transiently persisted and failed to give rise to new vessels. When we implanted cancer cells in different organs, the abortive angiogenic response in the heart resulted in a reduced expansion of the tumour mass. |
| **Conclusion** | Our genetic lineage tracing indicates that cardiac endothelial cells activate Apelin expression in response to pro-angiogenic stimuli but, different from those of the skeletal muscle, fail to proliferate and form mature and structured vessels. The poor angiogenic potential of the heart is associated with reduced tumour angiogenesis and growth of cancer cells. |

## Graphical Abstract

# 1. Introduction

It is common experience that heart ischaemia does not elicit an efficient angiogenic response, able to restore an appropriate supply of oxygen and nutrients to the hypoxic region. If not promptly revascularized, the infarcted myocardium inevitably heals by scarring, with detrimental consequences on heart function.[1] Various angiogenic factors are up-regulated early after ischaemia, indicating a spontaneous attempt of the heart to induce the formation of new blood vessels and revascularize the ischaemic region.[2,3] Yet, this process does not result in an efficient angiogenic response, consistent with the failure of clinical trials aimed at inducing therapeutic angiogenesis in the heart.[4,5] In addition, recent experimental evidence showed that collateral vessels after myocardial infarction are formed by arteriogenesis (i.e. the appearance of visible arteries from pre-existing small arterioles by rapid lumen opening and vascular wall thickening) and not by angiogenesis.[6]

Different from the heart, tumours have a remarkable capacity to form new blood vessels in response to hypoxia. During tumour growth, the central core becomes progressively hypoxic, inducing the expression of multiple angiogenic factors, among which the most potent is the vascular endothelial growth factor (VEGF). The *VEGF* gene encodes for a transcript that is alternatively spliced to produce multiple isoforms, each one characterized by different angiogenic potential.[4] The most potent isoform is the one composed by 165 amino acids (VEGF165),[7] herein referred to as VEGF. Tumour-derived VEGF potently promotes the formation of new capillaries, thus supporting the further growth of cancer cells.[8] The reasons why a hypoxic tumour efficiently induces an angiogenic response, leading to new blood vessel formation, whereas a hypoxic heart fails to do the same are currently not understood.

Our laboratory has a long-lasting interest in the use of vectors derived from the adeno-associated virus (AAV) for the induction of therapeutic angiogenesis through the delivery of VEGF. This strategy was very effective in promoting the massive formation of new blood vessels after either hind limb ischaemia, or other ischaemic diseases, in which the vector was delivered to the skeletal muscle.[9–12] However, when we applied the same approach to cardiac ischaemia, we have never observed any remarkable angiogenic response and eventually discovered a direct, protective effect of VEGF on cardiomyocytes, independent from angiogenesis.[13] In particular, the delivery of AAV-VEGF after myocardial infarction did not result in a significant endothelial cell proliferation and generation of new capillaries, however, we observed an increased number of arteries,[13,14] again consistent with ongoing arteriogenesis.[6]

To experimentally assess whether the skeletal and cardiac muscle differentially respond to angiogenic stimuli, we took advantage of a genetic lineage tracing approach, in which the Tamoxifen-inducible form of the Cre recombinase (CreER) is expressed under the control of the *Apelin* (*Apln*) promoter.[15] Apelin is a highly conserved secreted peptide, acting as the endogenous ligand for the human G protein-coupled receptor APJ.[16] Endothelial cells express abundant levels of Apelin during embryonic development, when angiogenesis is active in almost all organs, and markedly down-regulates its expression in adulthood, when they become quiescent.[15,17] However, in response to hypoxia, under tissue ischaemia or in the context of a tumour, Apelin expression is typically reactivated, particularly by tip cells, which induce stalk cell proliferation through Dll4/Notch1 signalling,[18,19] during sprouting angiogenesis.[17,20] Thus, the Apln-CreER mouse is a powerful tool to genetically label sprouting endothelial cells and their progeny.[6,15] Here, we take advantage of this mouse strain to analyse the response of cardiac and skeletal

muscle endothelial cells to pro-angiogenic stimuli and follow their fate in the two organs *in vivo*.

# 2. Methods

Extended materials and methods are provided as Supplementary material online.

## 2.1 AAV vector production and administration

All rAAV vectors were produced by the AAV Vector Unit at ICGEB Trieste (https://www.icgeb.org/facilities/avu-core-facility/).[7] AAV9 (herein referred to as AAV) vectors were injected into either the tibialis anterior muscle or the left ventricular wall of the adult heart using a 30G syringe.[7,21]

## 2.2 DNA and RNA extraction and quantification

Total DNA was isolated using the DNeasy Blood and Tissue Kit to detect and quantify vector DNA by real-time PCR.[21] Total RNA was isolated using TRIzol Reagent. Reverse transcription was performed using First Strand cDNA Synthesis Kit with random primers. The expression of *VEGF* and *Gapdh* was detected using specific primers and TaqMan® probes, while the expression of *Notch1*, *Hes1*, and *Hey* was detected using SYBR Green.

## 2.3 Protein extraction and VEGF quantification

Proteins were extracted from the skeletal and cardiac muscle using RIPA buffer supplemented with protease inhibitors. The amount of mouse and human VEGF were quantified using Mouse VEGF Quantikine ELISA (R&D systems) and VEGF human ELISA (Abcam) kits. Data were normalized on protein content.

## 2.4 Mice

All animal experiments were conducted in accordance with guidelines from the Directive 2010/63/EU of the European Parliament on animal experimentation in compliance with European guidelines and International Laws and Policies (EC Council Directive 86/609, OJL 34, 12 December 1987). CD1, Balb/c, and C57BL/6 mice were purchased from Harlan Laboratories. Adult AplnCreER[6] mice were crossed with Rosa26-mT/mG mice[22] to obtain AplnCreER; Rosa26-mT/mG animals. To activate Cre-mediated recombination, 4-hydroxytamoxifen was dissolved in corn oil and injected intraperitoneally. To label proliferating cells, 5-ethynyl-2′-deoxyuridine (EdU) was administered intraperitoneally.

B16-F10 melanoma and LG1233 lung adenocarcinoma cells were injected into C57BL/6 mice either into the tibialis anterior skeletal muscle or the left ventricular wall of the heart. Breast cancer 4T1cells were injected into Balb/c mice. B16-F10 and 4T1 cells were also injected subcutaneously into the right flank. Tumour volume was measured using the formula: $V = \pi/6*(d_{max}^2 * d_{min}/2)$.[23]

Mice were anaesthetized with 1% isoflurane for intramuscular injections and with ketamine–xylazine (100–40 mg/kg) for intracardiac injections. At the end of the experiment, mice were anaesthetized with 5% isoflurane and euthanized by cervical dislocation.

## 2.5 Primary endothelial cell cultures and spheroids

Endothelial cells were selected by magnetic separation and plated in primary 96-well plates coated with fibronectin/gelatin in EGM-2 medium. For Apelin expression assay, cells were cultured in the presence of both 4-hydroxytamoxifen and recombinant human VEGF. For endothelial spheroid formation, cells were seeded into agarose-coated round bottom plates. Spheroids were transferred on top of a collagen layer and cultured in EGM-2 medium supplemented with 4-hydroxytamoxifen to allow endothelial cell sprouting and EGFP expression.

## 2.6 Western blot

Protein lysates were run in 10% polyacrylamide gels and transferred to nitrocellulose membranes probed with the following antibodies: VEGFR2 (Santa Cruz Biotechnology, sc-504), Akt1 (Cell Signaling Technology, 2938), phospho-Akt (Cell Signaling Technology, 4056), Erk1/2 (Cell Signaling Technology, 9102), phospho-Erk1/2 (Santa Cruz Biotechnology, sc-136521), tubulin (Merck, T5168), and β-actin (Merck, A3854).

## 2.7 Immunofluorescence, image acquisition and analysis

Hearts and skeletal muscles were fixed in paraformaldehyde (PFA) and equilibrated in sucrose before embedding in OCT and cryosectioning. Sections were transferred on microslides, permeabilized in Triton X-100, blocked in BSA and incubated with primary antibodies. Cells were fixed in PFA, permeabilized, blocked, and incubated with primary antibodies. Alexa Fluor-conjugated secondary antibodies were used to detect primary antibodies, while nuclei were counterstained with Hoechst. EdU incorporation was visualized using the EdU Click-iT assay. Images were acquired using a Nikon fluorescent microscope, a Zeiss LSM 880 confocal microscope and analysed using ImageJ2 software.[24] Three-dimensional rendering of 100 μm thick sections were obtained using Surface module of Imaris (Bitplane).

## 2.8 Flow cytometry and cell sorting

Samples were stained using antibodies specific for CD31, Dll4, VEGFR1, and CD45. Cells were acquired using a FACSCelesta and sorted using a FACS Aria II (BD).

## 2.9 Statistical analysis

Statistical analysis was performed using Excel and GraphPad Prism 7.0 on data expressed as mean ± standard error. Unpaired Student's *t*-test and one-way analysis of variance (ANOVA) with Student–Newman–Keuls correction were used to determine statistical significance for the normally distributed datasets, whereas non-normally distributed datasets were analysed by ANOVA on ranks and Mann–Whitney *U* test. *P*-value <0.05 was considered significant.

# 3. Results

## 3.1 The cardiac muscle is less responsive to VEGF than the skeletal muscle

To analyse the angiogenic response elicited by VEGF in either the skeletal or cardiac muscle, we injected the same dose of AAV-VEGF into the tibialis anterior and the left ventricular wall of 8 weeks old CD1 mice, using an empty AAV vector as a control (AAV-control). Animals were

injected with the thymidine analogue EdU every other day starting from Day 14 after vector administration, to specifically assess the proliferative response of endothelial cells to VEGF. All animals were eventually sacrificed at Day 30 for molecular and histological evaluation, as schematically represented in *Figure 1A*. As expected, the number of AAV viral genomes was comparable in the two tissues (*Figure 1B*) and this resulted also in comparable levels of both human *VEGF* mRNA and protein in both tissues (*Figure 1C and D*).

Consistent with previous data,[7,9] we found that VEGF-induced massive formation of new $\alpha$-SMA$^+$ arterioles (with a diameter in the 20–200 µm range) in the skeletal muscle. While the AAV-MCS-injected muscle contained $4 \pm 0.25$ arterial vessels per field, this number raised up to $13.7 \pm 1.1$ upon the injection of AAV-VEGF. In contrast, the increase in the number of arterial vessels was modest in the heart ($4.8 \pm 0.2$ and $6.3 \pm 0.8$ arteries per field in response to AAV-control and AAV-VEGF, respectively). Similar results were obtained by quantifying the number of pixels corresponding to $\alpha$-SMA$^+$ signal, as shown in *Figure 1E and G*. The difference in the number of capillaries formed in response to VEGF in the two organs was even more evident. While the number of either CD31$^+$ (*Figure 1E and H*) or ERG$^+$ endothelial cells (*Figure 1F and I*) markedly increased upon AAV-VEGF injection in the skeletal muscle, no induction of angiogenesis was observed in the adult heart (*Figure 1E, F, H, and I*). In contrast, VEGF-induced angiogenesis was robust in neonatal hearts (Supplementary material online, *Figure S1A–G*).

By assessing EdU incorporation in endothelial cells, we observed a massive proliferative response of CD31$^+$ endothelial cells in the skeletal muscle and in the neonatal heart, but only a minimal effect in the adult heart (*Figure 1J and K* and Supplementary material online, *Figure S1H and I*).

Taken together, these results indicate that the response of endothelial cells to VEGF is blunted after birth in the heart, while it remains robust in the adult skeletal muscle.

## 3.2 VEGF induces sprouting angiogenesis in the skeletal but not in the cardiac muscle

To further characterize the angiogenic capacity of adult skeletal muscle and heart, we took advantage of a transgenic mouse enabling the genetic tracing of Apelin-expressing cells and their progeny (Apln-CreER; R26mT/mG). In this mouse, membrane-localized tdTomato is produced by all cells, while it switches to membrane-EGFP upon tamoxifen-inducible Cre recombination, occurring only in Apelin$^+$ cells. This mouse has been previously used to genetically label sprouting endothelial cells.[15]

We injected either AAV-VEGF or AAV-control in the skeletal muscle and heart of these mice, followed by tamoxifen administration at Days 1 and 7 (*Figure 2A*). Also in this mouse strain, VEGF overexpression resulted in an increased number of endothelial cells in the skeletal muscle but not in the heart, as detected by the two endothelial markers CD31 and ERG. In both muscle types, the fraction of Apelin$^+$ endothelial cells was significantly increased in response to VEGF, indicative of proper response to the growth factor at the individual cell level (*Figure 2B, C, and E*). These Apelin$^+$ cells were incorporated in the VEGF-induced arterioles in the skeletal muscle, but not in the heart (*Figure 2D and F*). Apelin$^+$ cells were negative for the pan-leukocytic marker CD45 (Supplementary material online, *Figure S2*), consistent with their endothelial identity.

To assess whether cardiac endothelial cells were able to respond to a higher dose of VEGF, we injected a 100-fold concentrated viral preparation (Supplementary *Figure S3A*) in either the heart or the skeletal muscle

of Apln-CreER; R26mT/mG mice. We did not detect any increase in the number of arteries containing EGFP$^+$ endothelial cells in any of the two organs compared with the initial concentration of the virus (compare *Figure 2D* with Supplementary material online, *Figure S3B and D*). On the other hand, a 100-fold diluted preparation did not elicit any angiogenic response in any muscle type (Supplementary material online, *Figure S3C and D*).

Thus, VEGF is sensed by endothelial cells in both skeletal and cardiac muscle. In the latter tissue, however, it fails to induce further steps of angiogenesis and Apelin$^+$ cells do not contribute to the formation of arterioles.

## 3.3 Tumour cell-induced angiogenesis is impaired in the heart

We wondered whether the response to other angiogenic stimuli might also be impaired in the adult heart. In particular, we investigated cancer-associated angiogenesis, knowing that the heart is one of the exceptional organs in the body in which both primary and secondary tumours are extremely rare.[25] By taking advantage of the documented capacity of Apln-CreER; R26mT/mG mice to label sprouting endothelial cells within tumours,[15] we implanted lung cancer LG cells in either the tibialis anterior or the left ventricle of these mice, followed by tamoxifen administration at Days 1 and 4. Animals were sacrificed at Day 3, 6, and 9 after tumour cell injection for histological evaluation of angiogenesis (*Figure 3A*). Within the tumours implanted in the skeletal muscle, the number of EGFP$^+$CD31$^+$ endothelial cells progressively increased over time, resulting markedly higher at Day 9 compared with the surrounding, healthy tissue. In contrast, in the heart, endothelial cells switched on Apelin expression early after cancer cell implantation, but the number of these cells within the tumour area progressively decreased, becoming similar to that found in the surrounding, non-infiltrated myocardium at Day 9 (quantification in *Figure 3B* and representative images at Day 9 in*Figure 3D*; images of the entire time course are in Supplementary material online, *Figure S4A*).

Next, we wondered whether the progressive decrease in the number of Apelin$^+$ endothelial cells in tumour-implanted hearts could be due to their death. By staining tissue sections for the apoptosis marker cleaved Caspase-3, we observed the presence of numerous apoptotic EGFP$^+$ cells, particularly evident at Day 6 after cancer cell implantation in the heart (representative images and quantification in Supplementary material online, *Figure S5*). No apoptotic cells were detected in the skeletal muscle.

In the same samples, the number of EGFP$^+$ arterioles in the skeletal muscle significantly increased over time in the tumour region compared with the surrounding, non-infiltrated tissue (quantification in *Figure 3C* and representative images at Day 9 in *Figure 3E*; images of the entire time course are in Supplementary material online, *Figure S4B*). In contrast, very few EGFP$^+$ arteries were detected in the heart, either within tumours or in the surrounding area (*Figure 3C and E*).

These results reiterate that, similar to what we observed in response to AAV-VEGF, cancer cells induce Apelin expression in endothelial cells of both skeletal muscle and heart, but in the latter organ Apelin$^+$ cells die and do not become incorporated into the cancer-associated vessels.

To investigate whether the different angiogenic capacity of skeletal muscle and heart might impact on tumour cell survival and proliferation, we monitored LG tumour volume over time. We found that cancer cells grew at a slower rate in the cardiac than in the skeletal muscle at all analysed time points (*Figure 4A*). This marked difference was attributable to
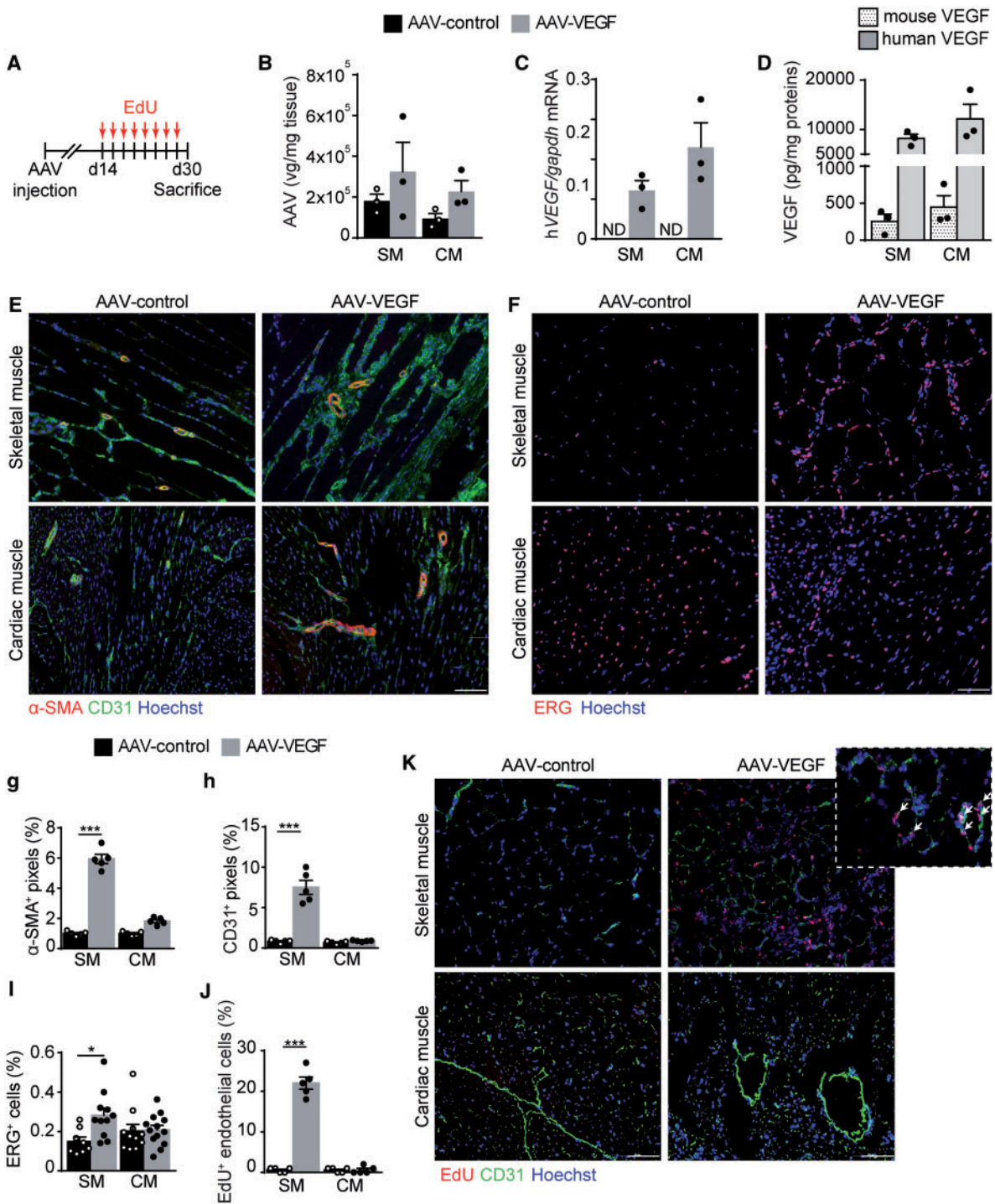
**Figure 1** VEGF induces a potent angiogenic response in the skeletal but not in the cardiac muscle. (A) Schematic of the AAV and EdU injection. (B) Real-time PCR quantification of the number of AAV viral genomes (vg) in the skeletal muscle (SM) and cardiac muscle (CM) normalized on tissue weight. (C) Real-time PCR quantification of human *VEGF* mRNA normalized on mouse *GAPDH*. (D) Quantification of mouse and human VEGF by ELISA assay normalized on tissue weight. (E) Representative immunofluorescence staining of skeletal and cardiac muscle, injected with either AAV-control (left) or AAV-VEGF (right), using anti-α-SMA and anti-CD31 antibodies. (F) Representative immunofluorescence staining of skeletal and cardiac muscle, injected with either AAV-control (left) or AAV-VEGF (right), using anti-ERG antibodies. (G) Quantification of the area covered by α-SMA$^+$ cells. (H) Quantification of the area covered by CD31$^+$ cells. (I) Quantification of the percentage of ERG$^+$ nuclei. (J) Quantification of the percentage of EdU$^+$ CD31$^+$ cells. (K) Representative immunofluorescence staining of skeletal and cardiac muscle, injected with either AAV-control (left) or AAV-VEGF (right) showing EdU$^+$ nuclei and CD31$^+$ endothelial cells. The inset shows a higher magnification to visualize EdU$^+$CD31$^+$ endothelial cells (indicated by arrows). In *B–D*, *G–J* data are shown as mean ± S.E.M. Statistical significance was determined using a two-way ANOVA followed by Tukey's multiple comparison test, *$P < 0.05$, ***$P < 0.001$, $n = 3–5$ per group. Scale bar in *E*, *F*, and *K* 100 μm.
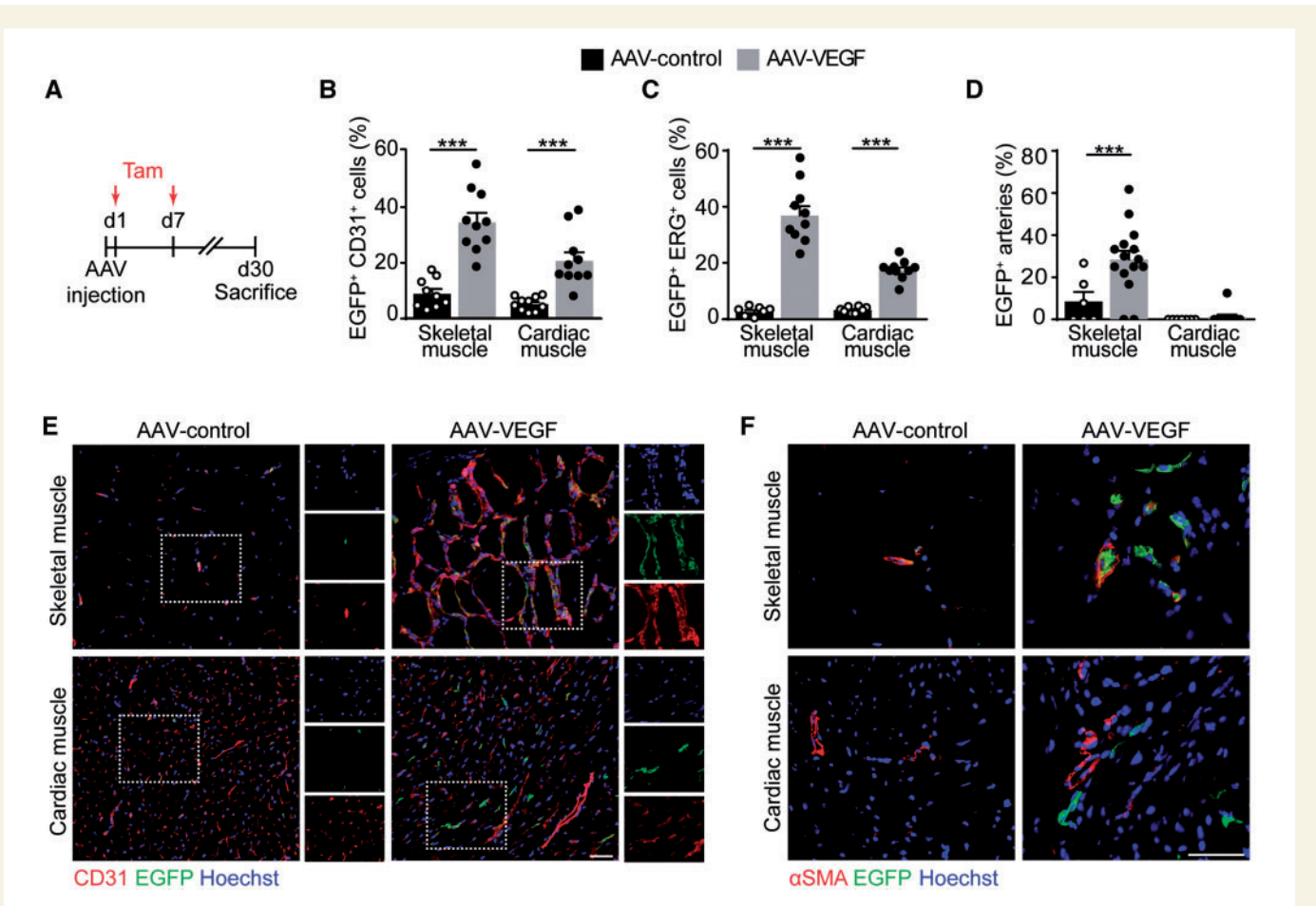
**Figure 2** Sprouting Apelin+ endothelial cells differentially contribute to the formation of arterial vessels in response to VEGF in the skeletal and cardiac muscle. (A) Schematic of AAV and tamoxifen (Tam) injection in Apln-CreER; R26mT/mG mice. (B) Quantification of the number of EGFP$^+$ CD31$^+$ endothelial cells (% of CD31$^+$ cells). (C) Quantification of the number of EGFP$^+$ ERG$^+$ endothelial cells (% of ERG$^+$ cells). (D) Quantification of the number of arteries containing EGFP$^+$ endothelial cells (% of total arteries). (E) Representative immunofluorescence staining of skeletal and cardiac muscle of Apln-CreER; R26mT/mG mice injected with either AAV-control (left) or AAV-VEGF (right), labelled with anti-CD31 antibodies. Boxed regions are shown as split channels in the panels on the right. (F) Representative immunofluorescence staining of skeletal and cardiac muscle of Apln-CreER; R26mT/mG mice injected with either AAV-control (left) or AAV-VEGF (right), labelled with anti-α-SMA antibodies. In (B–D) data are shown as mean ± S.E.M. Statistical significance was determined using a two-way ANOVA followed by Tukey's multiple comparison test, ***$P < 0.001$, $n \geq 7$ per group. Scale bar in E, F, 100 μm.

both reduced proliferation and increased apoptotic death of cancer cells in the heart, as shown by staining for the proliferation marker Ki67 and the apoptosis marker cleaved Caspase-3 (quantification in *Figure 4B* and *C* and representative images in *Figure 4D* and *E*).

We also wanted to confirm these findings using two additional cancer cell lines. We injected the same number of 4T1 breast cancer cells and B16-F10 melanoma cells into either the skeletal or cardiac muscle of syngeneic Balb/c and C57BL/6 mice, respectively. At 15 days, tumours were clearly detectable by gross examination of the injected organs. Representative pictures of control skeletal and cardiac muscles and the same organs injected with LG, B16-F10, and 4T1 cells are shown in *Figure 4F–I*. For all the tested cell lines, tumours formed in the skeletal muscle were invariably larger than those formed in the heart (*Figure 4J–L*) and similar to those implanted subcutaneously (Supplementary material online, *Figure S6*).

Collectively, these results are consistent with the conclusion that sprouting endothelial cells efficiently contribute to cancer-associated angiogenesis in the skeletal muscle, but fail to do so in the heart.

### 3.4 Cardiac endothelial cells sense the VEGF stimulus but fail to sprout *ex vivo*

Since we detected a similar expression of Apelin in both organs early after the angiogenic stimulus, we aimed at assessing the angiogenic potential of primary endothelial cells isolated from both tissues. First, we isolated endothelial cells from Apln-CreER; R26mT/mG mice and exposed them to both tamoxifen and VEGF for 48 h. Consistent with the *in vivo* results, we observed that both cell types activated Apelin expression in response to VEGF (*Figure 5A* and *B*). Next, we assessed their proliferation and found that the number of Ki67$^+$ cells isolated from the skeletal muscle significantly increased upon VEGF administration, while that of cardiac cells did not (*Figure 5C* and *D*). In both cases, proliferating endothelial cells were largely negative for Apelin (the percentage of Ki67$^+$ EGFP$^+$ cells was invariably lower than 0.05, as shown by representative images in Supplementary material online, *Figure S7A*). While we did not detect any major difference in the expression of the major pro-angiogenic receptor VEGFR2, downstream signalling pathways resulted
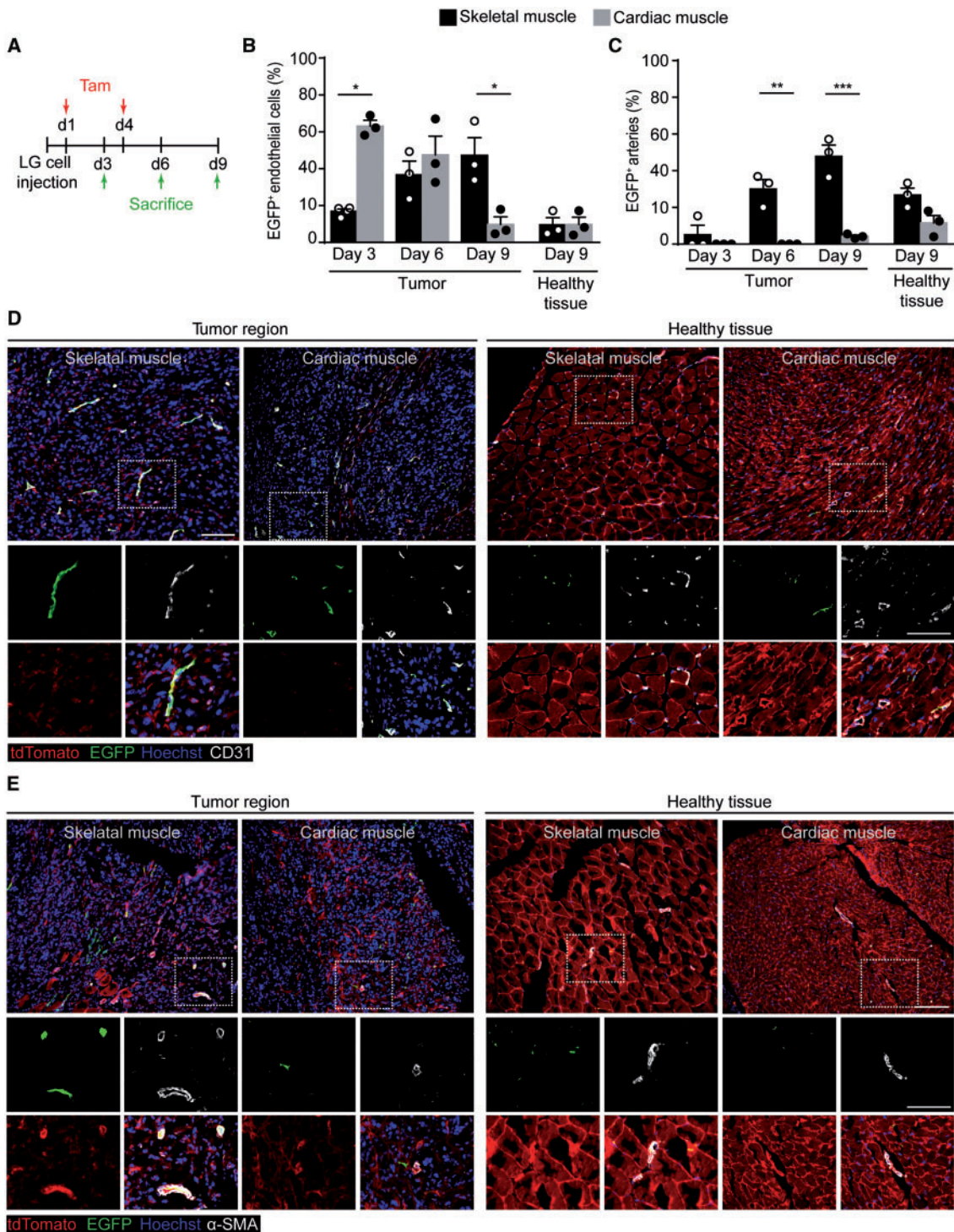
**Figure 3** Sprouting Apelin+ endothelial cells differentially contribute to tumour angiogenesis in the skeletal and cardiac muscle. (*A*) Schematic of LG cell and tamoxifen (Tam) injection in Apln-CreER; R26mT/mG mice. (*B*) Quantification of the number of EGFP+ endothelial cells (% of CD31+ cells) at the indicated time points in either the tumour region or the surrounding, healthy tissue. (*C*) Quantification of the number of arteries containing EGFP+ endothelial cells (% of total arteries) at the indicated time points in either the tumour region or the surrounding, healthy tissue. (*D*) Representative immunofluorescence staining of skeletal and cardiac muscle of Apln-CreER; R26mT/mG mice injected with LG cells, labelled with anti-CD31 antibodies 9 days after cancer cell injection. Panels on the left show regions highly infiltrated by cancer cells, whereas panels on the right show the surrounding, healthy tissue. Boxed regions are magnified in the lower panels to show split channels. (*E*) Representative immunofluorescence staining of skeletal and cardiac muscle of Apln-CreER; R26mT/mG mice injected with LG cells, labelled with anti-α-SMA antibodies 9 days after cancer cell injection. Panels on the left show regions highly infiltrated by cancer cells, whereas panels on the right show the surrounding, healthy tissue. In (*B, C*) data are shown as mean ± S.E.M. Statistical significance was determined using a two-way ANOVA followed by Tukey's multiple comparison test, *$P < 0.05$, **$P < 0.01$, ***$P < 0.001$, $n = 3$ per group. Scale bar in *D, E* 200 μm.
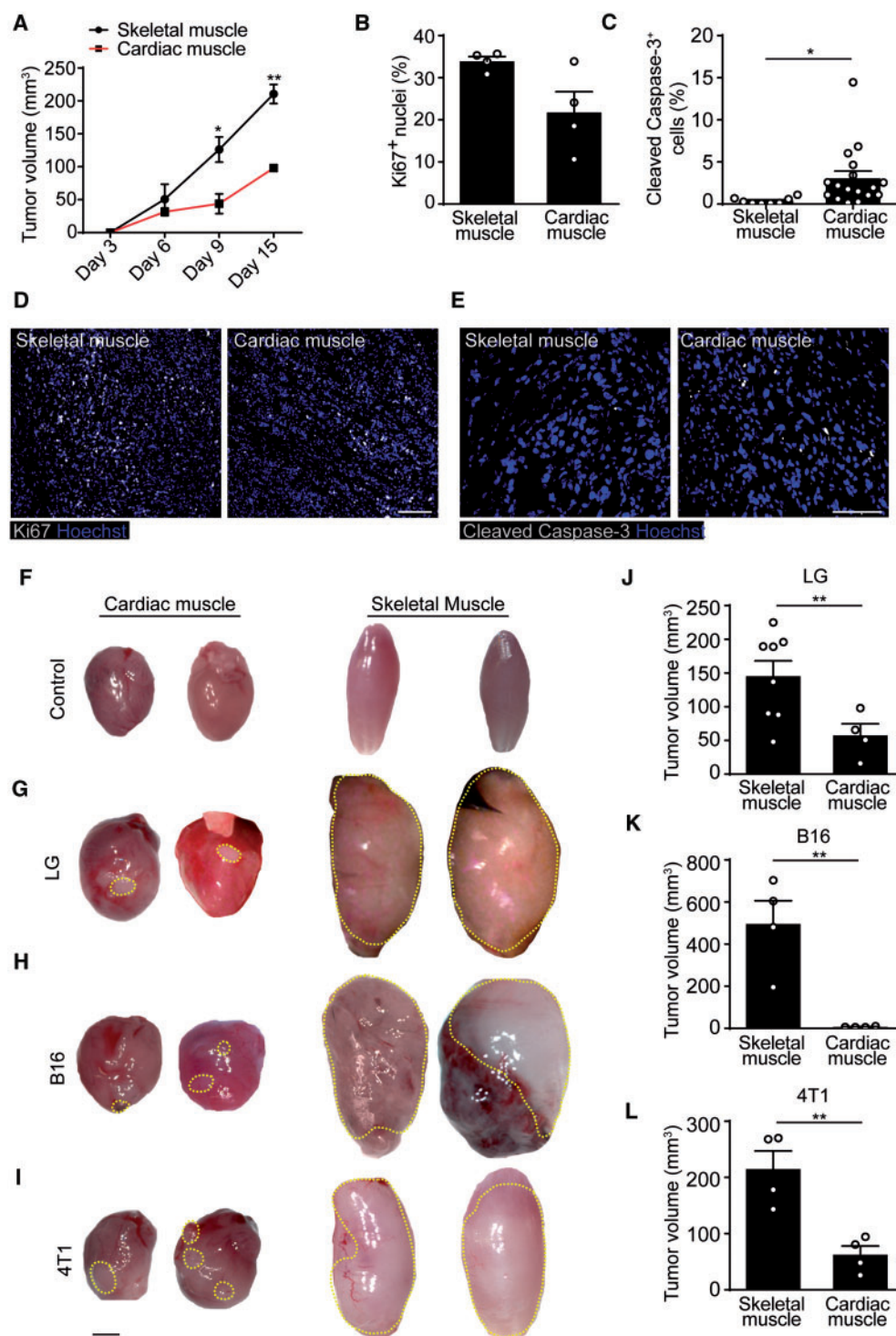
**Figure 4** Tumours grow less in the heart than in the skeletal muscle. (A) Quantification of tumour size at different time points after LG cell implantation into either the skeletal or the cardiac muscle. (B) Quantification of Ki67$^+$ nuclei (% of total nuclei) in sections of either skeletal or cardiac muscle at 10 days after LG cell implantation. (C) Quantification of cleaved Caspase-3$^+$ cells in sections of either skeletal or cardiac muscle at 10 days after LG cell implantation. (D) Representative immunofluorescence staining of skeletal and cardiac muscle injected with LG cells using anti-Ki67 antibodies. Scale bar, 100 μm. (E) Representative immunofluorescence staining of skeletal and cardiac muscle injected with LG cells using anti-cleaved Caspase-3 antibodies. Scale bar, 50 μm. (F–I) Representative whole organ pictures of hearts and skeletal muscle not treated (F) or injected with LG lung adenocarcinoma (G), B16/F10 melanoma (H), and 4T1 breast cancer cells (I). Tumour area is indicated by a dashed yellow line. Scale bar in F–I, 2 mm. (J–L) Quantification of LG (J), B16 (K), and 4T1 (L) tumour size in skeletal and cardiac muscle at 10 days after cell implantation. In A–C, J–L data are shown as mean ± S.E.M. Statistical significance was determined using a two-way ANOVA followed by Tukey's multiple comparison test for data in A, and by Student's t-test in B, C, J, K, L, *P < 0.05, **P < 0.01, n ≥ 4 per group.
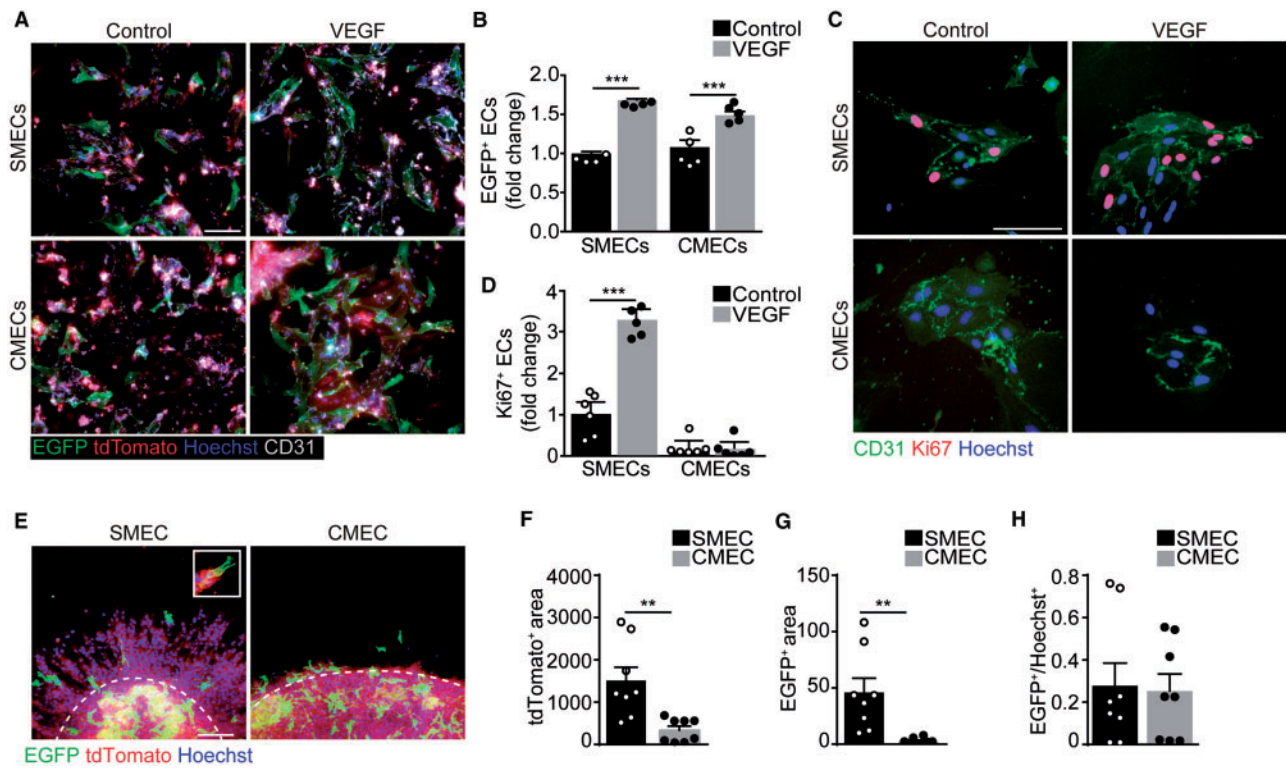
**Figure 5** Cardiac endothelial cells up-regulate Apelin but fail to form vascular structures upon VEGF stimulation *in vitro*. (*A*) Representative images of cultured skeletal muscle and cardiac endothelial cells (SMECs and CMECs, respectively) isolated from Apln-CreER; R26mT/mG mice, treated with tamoxifen, either in the presence or in the absence of VEGF (100 ng/mL) for 48 h. Endothelial cells are labelled with anti-CD31 antibodies. (*B*) Quantification of EGFP$^+$ endothelial cells (percentage of CD31$^+$ cells). (*C*) Representative images of SMECs and CMECs isolated from C57Bl/6 mice either in the presence or in the absence of VEGF (100 ng/mL) for 48 h. Endothelial cells are labelled with anti-CD31 antibodies and proliferating cells with anti-Ki67 antibodies. (*D*) Quantification of Ki67$^+$ endothelial cells (percentage of CD31$^+$ cells). (*E*) Representative images of SMEC and CMEC spheroids isolated from Apln-CreER; R26mT/mG mice and let to sprout for 48 h. The boundary between the spheroid body and the sprouts is marked with a dashed white line. The inset shows an EGFP$^+$ cell, presenting numerous filopodia classically associated to tip cells, at the forefront of a growing sprout. (*F* and *G*) Quantification of tdTomato$^+$ (*F*) and EGFP$^+$ (*G*) area in the sprouts (normalized to the length of the spheroid boundary visible in each field). (*H*) Quantification of EGFP$^+$ area within SMEC and CMEC spheroid body (EGFP$^+$/Hoechst$^+$ area). In *B*, *D*, *F*–*H* data are shown as mean ± S.E.M. Statistical significance was determined using a two-way ANOVA followed by Tukey's multiple comparison test for data in *B* and *D*, and by Student's *t*-test in *F*, *G*, *H*, \*\**P* < 0.01, \*\*\**P* < 0.001, *n* ≥ 4 per group. Scale bar in *A*, *C*, *E* 100 μm.

more active in basal conditions in endothelial cells derived from the skeletal muscle compared with those derived from the heart. Phosphorylation of both Akt and Erk1/2 tended to further increase in skeletal muscle, but not in cardiac endothelial cells, stimulated with VEGF in culture, consistent with their different proliferative potential (Supplementary material online, *Figure S7B–F*).

We also cultured the same cells in non-adhesive round bottom plates favouring their organization into spheroids, which were eventually transferred onto a collagen substrate to allow endothelial cell sprouting. Primary endothelial cells from skeletal muscle efficiently sprouted and formed tubular structures extending out of the spheroids over 2 days, while cardiac endothelial cells essentially remained inside the spheroid body and minimally migrated out of it (*Figure 5E* and *F*). Consistent with their higher sprouting capacity, muscle-derived spheroids contained a remarkable number of Apelin$^+$ cells in their sprouts (*Figure 5E* and *G*), often exhibiting the classic tip cell morphology (inset in *Figure 5E*). In contrast, cardiac endothelial spheroids contained numerous Apelin$^+$ cells in their bodies, similar to what was observed in muscle spheroids

(*Figure 5E* and *H*), but these cells were not able to sprout (*Figure 5E* and *G*).

Thus, endothelial cells from both muscle types respond to VEGF inducing Apelin expression, but those derived from the heart do not proliferate and are incapable of forming angiogenic sprouts in culture.

## 3.5 Apelin-positive endothelial cells fail to form elongated vascular structures in the heart in response to VEGF

Our data on cultured cells indicate that a comparable number of Apelin$^+$ cells is induced by VEGF in both skeletal and cardiac muscle, but they differentially proliferate and form vascular sprouts. We wondered whether similar differences were also occurring *in vivo* in the context of VEGF- and tumour-induced angiogenesis.

First, we focused on the capacity of Apelin$^+$ endothelial cells to form elongated vascular structures 30 days after AAV-VEGF injection in either skeletal or cardiac muscle of Apln-CreER; R26mT/mG mice (as schematically represented in *Figure 6A*). In control heart and skeletal muscle, the
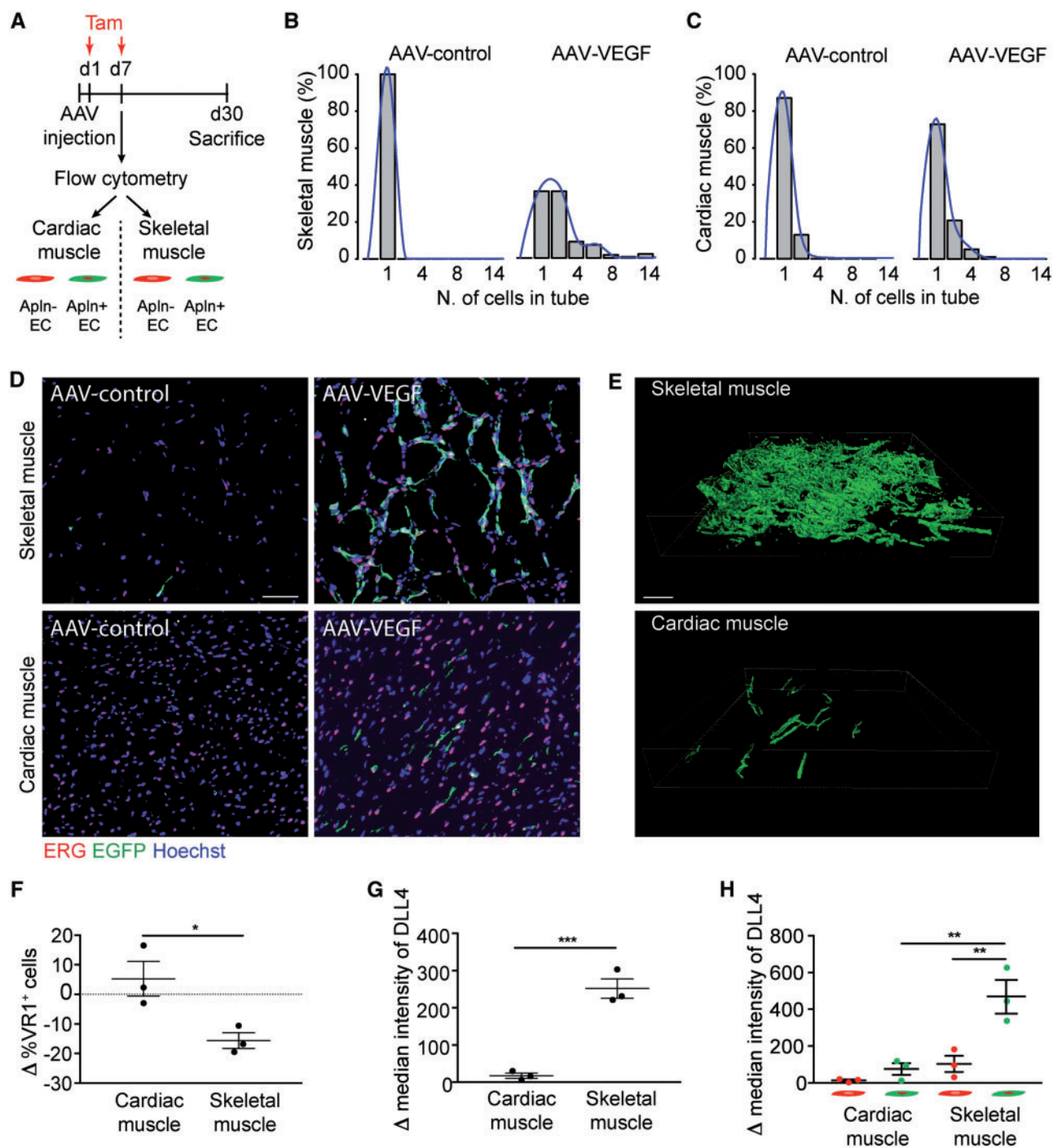
**Figure 6** Cardiac endothelial cells up-regulate Apelin but fail to form elongated vascular structures upon VEGF stimulation *in vivo*. (*A*) Schematic of AAV and tamoxifen (Tam) injection in Apln-CreER; R26mT/mG mice for characterization of sorted tdTomato$^+$ and EGFP$^+$ cells. (*B* and *C*) Histograms showing the number of EGFP$^+$ cells lining in a vascular tube in either skeletal (*B*) or cardiac (*C*) muscle injected with AAV-control (left) and AAV-VEGF (right). Superimposed to each histogram is the density plot (in blue). (*D*) Representative immunofluorescence staining of skeletal and cardiac muscle of Apln-CreER; R26mT/mG mice injected with either AAV-control or AAV-VEGF, labelled with anti-ERG antibodies. (*E*) Representative 3D renderings of 100 μm thick sections from skeletal and cardiac muscle of Apln-CreER; R26mT/mG mice injected with AAV-VEGF. (*F–H*) Flow cytometry analysis of CD31$^+$ VEGFR1(VR1)$^+$ cells (*F*) and DLL4 intensity in either total CD31$^+$ cells (*G*) or sorted tdTomato$^+$ and EGFP$^+$ cells (*H*), purified from cardiac and skeletal muscle of Apln-CreER; R26mT/mG mice, 7 days after AAV-VEGF injection. Data in *F–H* are shown as mean ± S.E.M. Statistical significance was determined using Student's *t*-test and one-way ANOVA followed by Tukey's multiple comparison test for data. *$P < 0.05$, **$P < 0.01$, ***$P < 0.001$. $n = 3$–6 per group. Scale bar in *D*, *E* 100 μm.

few EGFP$^+$ERG$^+$ endothelial cells were all individually spaced. Delivery of AAV-VEGF to the skeletal muscle resulted in a massive increase in the number of EGFP$^+$ERG$^+$ endothelial cells, which were often incorporated in elongated vascular structures, reaching up to 15 EGFP$^+$ERG$^+$ endothelial cells positioned in the same tube. In contrast, most of the EGFP$^+$ERG$^+$ endothelial cells in the heart remained as single cells or formed very short vascular structures, even after VEGF stimulation. The distribution of the number of EGFP$^+$ERG$^+$ endothelial cells in the same vascular tube is shown for both muscle types in *Figure 6B* and *C*, while representative images are shown in *Figure 6D*. Only in the skeletal muscle, this distribution was skewed towards the right in response to VEGF, indicating the generation of long capillaries by EGFP$^+$ERG$^+$ endothelial cells, while no significant changes could be observed in the heart. Comparable results were obtained in 100 µm thick muscle sections, that better show the three-dimensional organization of the vascular network (*Figure 6E*, Supplementary material online, *Figure S8A* and *Movies S1–S4*). In parallel, we also assessed the effect of a 100-fold higher or lower dose of vector, and again we did not detect any improvement in vessel length by increasing the dose of VEGF in any of the two muscle types (Supplementary material online, *Figure S3E*). The lowest dose of the vector did not result in any angiogenic response (Supplementary material online, *Figure S3F*).

To shed light on the molecular mechanisms underlying the poor elongation of vascular tubes in response to VEGF in the heart, we used flow cytometry to characterize the expression of VEGFR1 and Dll4, which are well known to regulate endothelial cell proliferation and the crosstalk between tip and stalk cells during sprouting angiogenesis.[19,26] We followed the gating strategy shown in Supplementary material online, *Figure S9A–C* to separately analyse EGFP$^+$ cells and tdTomato$^+$EGFP$^-$ cells (possibly representing tip and stalk cells, respectively). We found that the percentage of VEGFR1$^+$ endothelial cells was significantly decreased at Day 7 after AAV-VEGF injection in the skeletal muscle, but not in the heart (*Figure 6F*). In parallel, Dll4 was significantly more expressed in response to VEGF in endothelial cells purified from the muscle compared with those purified from the heart (*Figure 6G*). This up-regulation in the muscle was almost totally sustained by Apelin$^+$ cells, consistent with their possible tip cell function (*Figure 6H*). As a result of increased Notch signalling from tip cells, the Notch-target genes *Hes1*, *Hey1* and *Notch1* itself were more expressed by tdTomato$^+$EGFP$^-$ cells purified from the skeletal muscle compared with those purified from the heart (Supplementary material online, *Figure S9D–F*).

Thus, VEGF stimulates effective angiogenesis and the formation of elongated vascular structures, relying on Notch signalling, in the skeletal muscle, but fails to do the same in the heart.

## 3.6 Apelin-positive endothelial cells fail to form elongated vascular structures in the heart in response to cancer cell implantation

Next, we moved to the cancer model and assessed tumour vessels at 10 days after LG cell implantation (*Figure 7A*). In the skeletal muscle, vessels included up to nine EGFP$^+$ cells lining in a row in the same vascular tube inside the tumour area. In contrast, most of the cardiac vessels contained only one or two EGFP$^+$ cells. The results of this quantification are shown in *Figure 7B* and representative images in *Figure 7C*. A comparable pattern was observed in 100 µm thick sections (*Figure 7D*, Supplementary material online, *Figure S8B* and *Movies S5* and *S6*). Similar to what was observed upon VEGF overexpression, Apelin$^+$ cells were

able to persist and generate elongated vascular structures only in the context of cancers growing in the skeletal muscle, skewing the distribution to the right compared with the one observed in the heart (*Figure 7B*).

We also analysed the spatial localization of these cells. While EGFP$^+$ vessels were abundantly present within the central part of the tumour in the skeletal muscle, most of the EGFP$^+$ cells were concentrated in the healthy tissue surrounding the tumour mass in the heart. By quantifying the EGFP$^+$ area in the border region (as defined in methods), we found that in the heart most of the Apelin$^+$ cells were still present in the healthy portion of the border 10 days after tumour implantation. In the skeletal muscle, the same cells had already penetrated inside the neoplastic mass (quantification is shown in *Figure 7E* and representative images in *Figure 7F*). Thus, in the heart sprouting Apelin$^+$ endothelial cells have a low capability to form elongated vascular structures and penetrate the tumour mass, consistent with their apoptotic phenotype particularly evident at Day 6 (Supplementary material online, *Figure S5*).

Overall, these data support a model in which endothelial cells in both skeletal and cardiac muscle similarly start expressing Apelin in response to pro-angiogenic stimuli (i.e. VEGF or molecules secreted by cancer cells). In the skeletal muscle, Apelin$^+$ cells activate Notch signalling and drive the formation of new vascular sprouts, which are eventually incorporated into arterial vessels. In contrast, Apelin$^+$ cells in the heart persist for a short period of time, undergo apoptosis and fail to drive an efficient angiogenic response (*Figure 8*).

## 4. Discussion

The results presented in this work provide a definitive evidence that the adult mammalian heart has a low angiogenic potential. While in the skeletal muscle angiogenic stimuli induce Apelin expression in a few endothelial cells, which sprout and lead to the formation of mature new vessels, in the heart Apelin$^+$ cells are unable to support an efficient angiogenesis.

The poor angiogenic nature of the adult heart was suggested by our serendipitous observation that the presence of the same amount of VEGF in either the skeletal or the cardiac muscle resulted in a very different angiogenic response. While VEGF induced a massive increase in the number of both capillaries and small arteries in the skeletal muscle, in the heart it resulted in the formation of a modest number of new arteries, with almost null endothelial cell proliferation.

Thus, we used Apln-CreER; R26mT/mG mice to genetically trace sprouting endothelial cells and follow their fate upon administration of pro-angiogenic stimuli. Besides VEGF, which is the most potent and best characterized angiogenic molecule, we also exploited the capacity of cancer cells to secrete pro-angiogenic factors. In both cases, i.e. the injection of either AAV-VEGF or cancer cells, a comparable proportion of endothelial cells started expressing Apelin in both muscle types. These cells efficiently formed new capillaries and were incorporated into small arteries in the skeletal muscle, but not in the heart, in which VEGF-induced arterioles were essentially Apelin-negative. These data are consistent with those obtained by He *et al.*,[6] who used the same genetic model to assess the mechanism responsible for the formation of new vessels during embryonic development and after myocardial infarction. These investigators found that arteries appearing in the adult heart after ischaemia did not bear any Apelin$^+$ cells and concluded that new vessels can be formed in the ischaemic heart only through arteriogenesis, namely the expansion of pre-existing arterioles, and not true
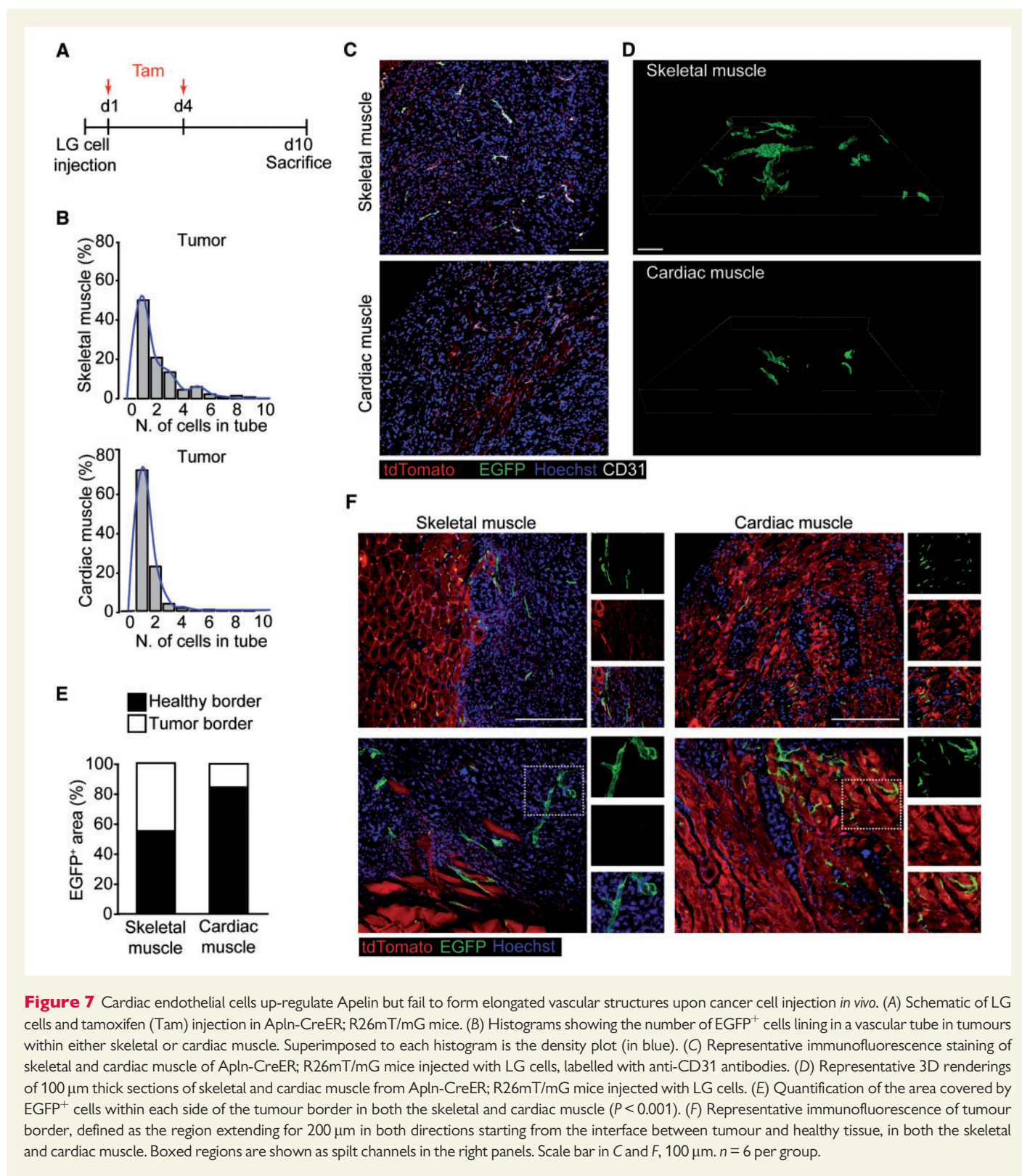
**Figure 7** Cardiac endothelial cells up-regulate Apelin but fail to form elongated vascular structures upon cancer cell injection *in vivo*. (*A*) Schematic of LG cells and tamoxifen (Tam) injection in Apln-CreER; R26mT/mG mice. (*B*) Histograms showing the number of EGFP^{+} cells lining in a vascular tube in tumours within either skeletal or cardiac muscle. Superimposed to each histogram is the density plot (in blue). (*C*) Representative immunofluorescence staining of skeletal and cardiac muscle of Apln-CreER; R26mT/mG mice injected with LG cells, labelled with anti-CD31 antibodies. (*D*) Representative 3D renderings of 100 μm thick sections of skeletal and cardiac muscle from Apln-CreER; R26mT/mG mice injected with LG cells. (*E*) Quantification of the area covered by EGFP^{+} cells within each side of the tumour border in both the skeletal and cardiac muscle (*P* < 0.001). (*F*) Representative immunofluorescence of tumour border, defined as the region extending for 200 μm in both directions starting from the interface between tumour and healthy tissue, in both the skeletal and cardiac muscle. Boxed regions are shown as spilt channels in the right panels. Scale bar in *C* and *F*, 100 μm. *n* = 6 per group.

angiogenesis.[6] Thus, the modest increase in the number of arterioles that we observed in the heart after AAV-VEGF administration can be reasonably ascribed to the recruitment and expansion of pre-existing vessels, in the absence of a true angiogenic response.

When we assessed the basal expression of Apelin in the two muscle types, we observed that the number of arteries containing Apelin[+]

endothelial cells was relatively higher in the untreated skeletal than in the cardiac muscle. Whether this indicates a spontaneous turnover of endothelial cells within arterial vessels in the skeletal muscle, which, different from the heart, is an organ endowed with a high regenerative capacity,[27] is an interesting hypothesis that requires further validation. Indeed, the different angiogenic capacity of the heart and the skeletal muscle well
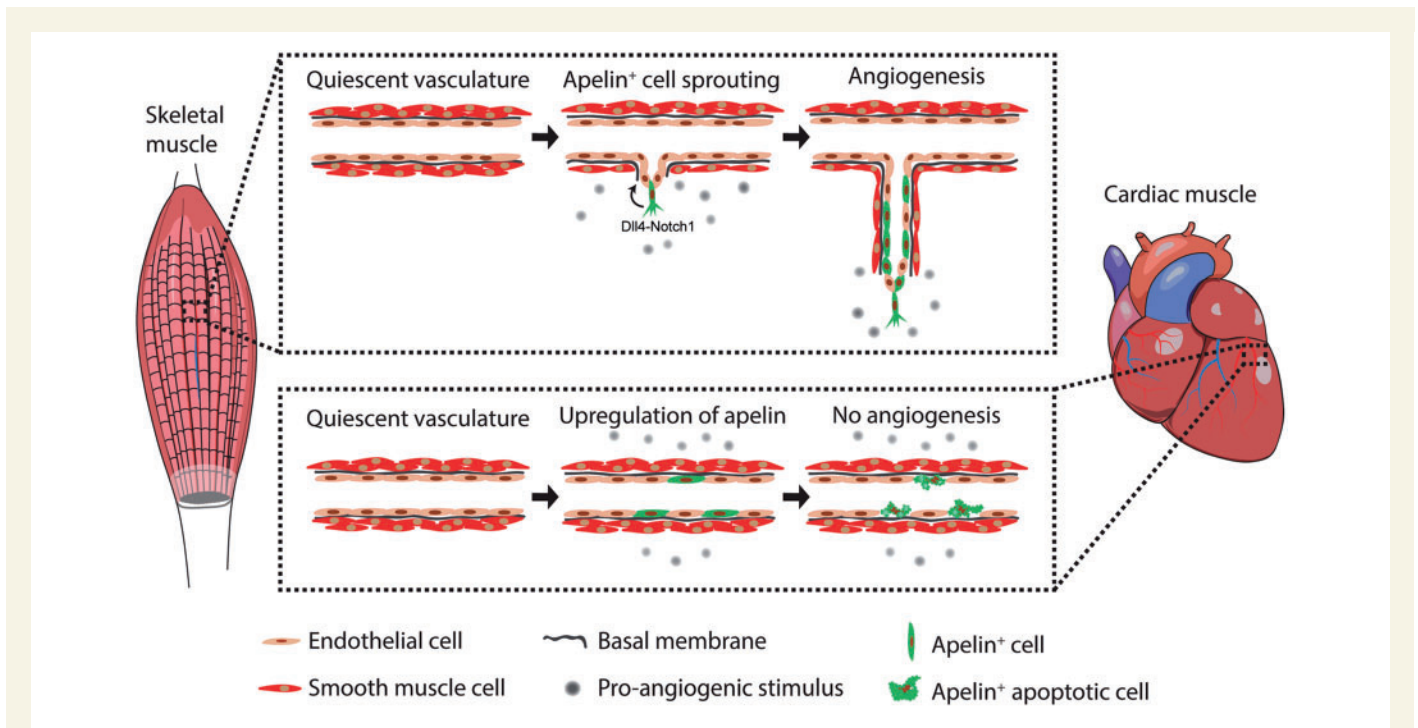
**Figure 8** Model showing the differential response of endothelial cells from the cardiac and skeletal muscle to pro-angiogenic stimuli. In response to a pro-angiogenic stimulus, such as VEGF or additional molecules secreted by cancer cells, a few endothelial cells in the skeletal muscle start expressing Apelin. These Apelin+ cells efficiently sprout, activate Dll4/Notch1 signalling and drive the formation of new vessels, to be eventually incorporated into arteries. In the heart, the same stimulus leads to a similar activation of Apelin in endothelial cells, which, however, only transiently persist and fail to form elongated vascular structures.

correlates with the different regenerative potential of the two muscle types. The regenerative response activated upon any kind of muscle injury entails massive activation of endothelial cells and profound remodelling of the vascular bed.[28] Angiogenesis and myogenesis are tightly coupled and controlled by a set of key molecules, including Periostin, Oncostatin M, and Apelin itself.[28] In contrast, the adult mammalian heart has a minimal, if not null, regenerative potential[29,30] and any damage is repaired by scarring. Lower vertebrates, such as fish and amphibians, are able to regenerate the myocardium after damage.[31] In these animals, endothelial cells invade the damaged area well before cardiomyocytes start proliferating, indicating that angiogenesis precedes and is possibly essential for heart regeneration.[32] The neonatal mammalian heart also retains some regenerative potential for a few days after birth,[33] yet the vascular network observed in the regenerating neonatal heart following apical resection is rather incomplete as compared with the normal myocardium,[34] again consistent with the poor capacity of the post-natal heart to form new arteries.

Previous studies claimed the effective formation of new blood vessels in response to VEGF and other angiogenic molecules in the heart of multiple species.[35] At a deeper analysis, most of these studies either used transgenic models, in which the angiogenic factor was active already during embryonic development, or they did not discriminate between spouting angiogenesis and other mechanisms of vessel formation. For instance, the cardiac-specific overexpression of another member of the VEGF family, VEGF-B, resulted in a massive angiogenic response in transgenic animals, but did not increase capillary density when delivered to adult hearts using AAV vectors.[36] In addition, many studies delivered the

angiogenic stimulus either using adenoviral vectors or recombinant proteins, both of which have a short half-life *in vivo* and exert a very transient effect.[37,38] This requires a very early analysis of the angiogenic response, which likely starts in the heart as in other organs, but fails to progress to form structured vessels. Indeed, we report that the pro-angiogenic stimulus is sensed by cardiac endothelial cells, as they do activate Apelin expression, and that the problem occurs at a later stage, during the vascular elongation phase.

Another difference between the two muscle types, is endothelial cell density, which appears higher in the heart compared with the skeletal muscle, when normalized per field. This difference is importantly reduced when the number of capillaries is normalized on the number of nuclei, as nuclei in the cardiac tissue are definitely denser than in the skeletal muscle. Thus, we would tend to exclude that the increased vessel density in the heart results in higher oxygenation and justifies the unresponsiveness of the cardiac muscle to VEGF, as also indicated by the comparable activation of Apelin expression in the two organs. Indeed, both muscle types up-regulated Apelin early after the injection of either VEGF or cancer cells, indicating that they are equally able to sense pro-angiogenic stimuli at the individual cell level. Increasing the dose of VEGF, by injecting a 100-fold more concentrated AAV vector, did not rescue the responsiveness of cardiac endothelial cells to angiogenic stimulation, nor increased the angiogenic response in the skeletal muscle, consistent with recent evidence that excessive VEGF stimulation does not result in functional angiogenesis.[39]

Apelin up-regulation was also observed in response to VEGF in primary endothelial cells, purified from both skeletal and cardiac muscle,

and grown *ex vivo* as either a monolayer or spheroids. While skeletal muscle-derived endothelial cells increased their proliferation and sprouting upon VEGF stimulation, cardiac endothelial cells did not increase their growth rate and failed to sprout from the spheroid body. Despite comparable levels of VEGFR2, downstream signalling was more active in cells purified from the skeletal muscle compared with those purified from the heart, both in basal conditions and upon VEGF stimulation. These data suggest that endothelial cells in both muscle types can specialize into tip cells, characterized by high levels of Apelin expression, and that a failure in the subsequent induction of stalk cell proliferation specifically occurs in cardiac endothelial cells. Consistently, in the skeletal muscle, the angiogenic process effectively proceeded and Apelin^{+} endothelial cells, along with their progeny, were incorporated into elongated vascular structures. In contrast, in the heart most of the Apelin^{+} endothelial cells stayed as single cells and died by apoptosis. When we followed their fate over time in the tumour model, we observed that these cells were mostly retained within the tumour border and failed to penetrate the neoplastic mass.

Can this poor angiogenic response be associated to the low incidence of cancer and metastasis in the heart? Primary and secondary cardiac tumours are indeed extremely uncommon,[40] despite the fact that the heart is among the most vascularized organs. Our results show that the experiential injection of cancer cells in the heart invariably resulted in poor cancer growth and inefficient angiogenesis.

Understanding the mechanisms blocking angiogenesis in the heart could thus offer novel opportunities for both interfering with cancer growth and promoting cardiac revascularization. We provide evidence that VEGFR1 and Dll4/Notch1 signalling are differentially regulated in endothelial cells purified from either the skeletal or the cardiac muscle, previously stimulated with VEGF. This could reflect a defective tip-to-stalk cell communication specifically occurring in the heart. Alternatively, the mechanism behind vessel elongation could be organ-specific and the traditional model of Notch1-dependent tip-to-stalk cell signalling, described in the retina, may not be necessarily applicable to other tissues. Our findings provide the base and experimental models for future investigation, aimed at clarifying the organotypic features of cardiac angiogenesis and their possible therapeutic exploitation.

# Supplementary material

Supplementary material is available at *Cardiovascular Research* online.

# Authors' contributions

T.K., M.R., A.Co., N.V., G.Z., A.Ca. performed most of the experiments. E.G. and G.M.P. performed flow cytometry and cell sorting. M.L. contributed to image analysis of tumour models. S.V. performed *in vivo* experiments. Z.B., F.B., M.H., M.G., and R.A. provided genetic models, reagents and critically discussed the experiments. L.Z. produced AAV vectors. T.K., A.Co., and S.Z. conceived the work and wrote the manuscript.

# References

1. Vogt A, von Essen R, Tebbe U, Feuerer W, Appel KF, Neuhaus KL. Impact of early perfusion status of the infarct-related artery on short-term mortality after thrombolysis for acute myocardial infarction: retrospective analysis of four German multicenter studies. *J Am Coll Cardiol* 1993;**21**:1391–1395.
2. Rivard A, Fabre JE, Silver M, Chen D, Murohara T, Kearney M, Magner M, Asahara T, Isner JM. Age-dependent impairment of angiogenesis. *Circulation* 1999;**99**:111–120.
3. Thiagarajan H, Thiyagamoorthy U, Shanmugham I, Dharmalingam Nandagopal G, Kaliyaperumal A. Angiogenic growth factors in myocardial infarction: a critical appraisal. *Heart Fail Rev* 2017;**22**:665–683.
4. Giacca M, Zacchigna S. VEGF gene therapy: therapeutic angiogenesis in the clinic and beyond. *Gene Ther* 2012;**19**:622–629.
5. Yla-Herttuala S, Bridges C, Katz MG, Korpisalo P. Angiogenic gene therapy in cardiovascular diseases: dream or vision? *Eur Heart J* 2017;**38**:1365–1371.
6. He L, Liu Q, Hu T, Huang X, Zhang H, Tian X, Yan Y, Wang L, Huang Y, Miquerol L, Wythe JD, Zhou B. Genetic lineage tracing discloses arteriogenesis as the main mechanism for collateral growth in the mouse heart. *Cardiovasc Res* 2016;**109**: 419–430.
7. Zacchigna S, Pattarini L, Zentilin L, Moimas S, Carrer A, Sinigaglia M, Arsic N, Tafuro S, Sinagra G, Giacca M. Bone marrow cells recruited through the neuropilin-1 receptor promote arterial formation at the sites of adult neoangiogenesis in mice. *J Clin Invest* 2008;**118**:2062–2075.
8. Carmeliet P, Jain RK. Molecular mechanisms and clinical applications of angiogenesis. *Nature* 2011;**473**:298–307.
9. Arsic N, Zentilin L, Zacchigna S, Santoro D, Stanta G, Salvi A, Sinagra G, Giacca M. Induction of functional neovascularization by combined VEGF and angiopoietin-1 gene transfer using AAV vectors. *Mol Ther* 2003;**7**:450–459.
10. Tafuro S, Ayuso E, Zacchigna S, Zentilin L, Moimas S, Dore F, Giacca M. Inducible adeno-associated virus vectors promote functional angiogenesis in adult organisms via regulated vascular endothelial growth factor expression. *Cardiovasc Res* 2009;**83**: 663–671.
11. Zacchigna S, Papa G, Antonini A, Novati F, Moimas S, Carrer A, Arsic N, Zentilin L, Visintini V, Pascone M, Giacca M. Improved survival of ischemic cutaneous and musculocutaneous flaps after vascular endothelial growth factor gene transfer using adeno-associated virus vectors. *Am J Pathol* 2005;**167**:981–991.
12. Zacchigna S, Tasciotti E, Kusmic C, Arsic N, Sorace O, Marini C, Marzullo P, Pardini S, Petroni D, Pattarini L, Moimas S, Giacca M, Sambuceti G. *In vivo* imaging shows abnormal function of vascular endothelial growth factor-induced vasculature. *Hum Gene Ther* 2007;**18**:515–524.
13. Zentilin L, Puligadda U, Lionetti V, Zacchigna S, Collesi C, Pattarini L, Ruozi G, Camporesi S, Sinagra G, Pepe M, Recchia FA, Giacca M. Cardiomyocyte VEGFR-1 activation by VEGF-B induces compensatory hypertrophy and preserves cardiac function after myocardial infarction. *FASEB J* 2010;**24**:1467–1478.
14. Ferrarini M, Arsic N, Recchia FA, Zentilin L, Zacchigna S, Xu X, Linke A, Giacca M, Hintze TH. Adeno-associated virus-mediated transduction of VEGF165 improves cardiac tissue viability and functional recovery after permanent coronary occlusion in conscious dogs. *Circ Res* 2006;**98**:954–961.
15. Liu Q, Hu T, He L, Huang X, Tian X, Zhang H, He L, Pu W, Zhang L, Sun H, Fang J, Yu Y, Duan S, Hu C, Hui L, Zhang H, Quertermous T, Xu Q, Red-Horse K, Wythe JD, Zhou B. Genetic targeting of sprouting angiogenesis using Apln-CreER. *Nat Commun* 2015;**6**:6020.
16. Charo DN, Ho M, Fajardo G, Kawana M, Kundu RK, Sheikh AY, Finsterbach TP, Leeper NJ, Ernst KV, Chen MM, Ho YD, Chun HJ, Bernstein D, Ashley EA, Quertermous T. Endogenous regulation of cardiovascular function by apelin-APJ. *Am J Physiol Heart Circ Physiol* 2009;**297**:H1904–H1913.
17. Kalin RE, Kretz MP, Meyer AM, Kispert A, Heppner FL, Brandli AW. Paracrine and autocrine mechanisms of apelin signaling govern embryonic and tumor angiogenesis. *Dev Biol* 2007;**305**:599–614.
18. Blanco R, Gerhardt H. VEGF and Notch in tip and stalk cell selection. *Cold Spring Harb Perspect Med* 2013;**3**:a006569.
19. Jakobsson L, Franco CA, Bentley K, Collins RT, Ponsioen B, Aspalter IM, Rosewell I, Busse M, Thurston G, Medvinsky A, Schulte-Merker S, Gerhardt H. Endothelial cells dynamically compete for the tip cell position during angiogenic sprouting. *Nat Cell Biol* 2010;**12**:943–953.
20. del Toro R, Prahst C, Mathivet T, Siegfried G, Kaminker JS, Larrivee B, Breant C, Duarte A, Takakura N, Fukamizu A, Penninger J, Eichmann A. Identification and functional analysis of endothelial tip cell-enriched genes. *Blood* 2010;**116**:4025–4033.
21. Eulalio A, Mano M, Ferro MD, Zentilin L, Sinagra G, Zacchigna S, Giacca M. Functional screening identifies miRNAs inducing cardiac regeneration. *Nature* 2012; **492**:376–381.
22. Muzumdar MD, Tasic B, Miyamichi K, Li L, Luo L. A global double-fluorescent Cre reporter mouse. *Genesis* 2007;**45**:593–605.

23. Carrer A, Moimas S, Zacchigna S, Pattarini L, Zentilin L, Ruozi G, Mano M, Sinigaglia M, Maione F, Serini G, Giraudo E, Bussolino F, Giacca M. Neuropilin-1 identifies a subset of bone marrow Gr1- monocytes that can induce tumor vessel normalization and inhibit tumor growth. *Cancer Res* 2012;**72**:6371–6381.

24. Rueden CT, Schindelin J, Hiner MC, DeZonia BE, Walter AE, Arena ET, Eliceiri KW. ImageJ2: imageJ for the next generation of scientific image data. *BMC Bioinformatics* 2017;**18**:529.

25. Ren DY, Fuller ND, Gilbert SAB, Zhang Y. Cardiac tumors: clinical perspective and therapeutic considerations. *Curr Drug Targets* 2017;**18**:1805–1809.

26. Lobov IB, Renard RA, Papadopoulos N, Gale NW, Thurston G, Yancopoulos GD, Wiegand SJ. Delta-like ligand 4 (Dll4) is induced by VEGF as a negative regulator of angiogenic sprouting. *Proc Natl Acad Sci USA* 2007;**104**:3219–3224.

27. Feige P, Brun CE, Ritso M, Rudnicki MA. Orienting muscle stem cells for regeneration in homeostasis, aging, and disease. *Cell Stem Cell* 2018;**23**:653–664.

28. Latroche C, Weiss-Gayet M, Muller L, Gitiaux C, Leblanc P, Liot S, Ben-Larbi S, Abou-Khalil R, Verger N, Bardot P, Magnan M, Chrétien F, Mounier R, Germain S, Chazaud B. Coupling between myogenesis and angiogenesis during skeletal muscle regeneration is stimulated by restorative macrophages. *Stem Cell Reports* 2017;**9**:2018–2033.

29. Giacca M, Zacchigna S. Harnessing the microRNA pathway for cardiac regeneration. *J Mol Cell Cardiol* 2015;**89**:68–74.

30. Zacchigna S, Giacca M. Extra- and intracellular factors regulating cardiomyocyte proliferation in postnatal life. *Cardiovasc Res* 2014;**102**:312–320.

31. Poss KD, Wilson LG, Keating MT. Heart regeneration in zebrafish. *Science* 2002;**298**:2188–2190.

32. Marin-Juez R, Marass M, Gauvrit S, Rossi A, Lai SL, Materna SC, Black BL, Stainier DY. Fast revascularization of the injured area is essential to support zebrafish heart regeneration. *Proc Natl Acad Sci USA* 2016;**113**:11237–11242.

33. Porrello ER, Mahmoud AI, Simpson E, Hill JA, Richardson JA, Olson EN, Sadek HA. Transient regenerative potential of the neonatal mouse heart. *Science* 2011;**331**:1078–1080.

34. Andersen DC, Ganesalingam S, Jensen CH, Sheikh SP. Do neonatal mouse hearts regenerate following heart apex resection? *Stem Cell Rep* 2014;**2**:406–413.

35. Zacchigna S, Zentilin L, Giacca M. Adeno-associated virus vectors as therapeutic and investigational tools in the cardiovascular system. *Circ Res* 2014;**114**:1827–1846.

36. Kivela R, Bry M, Robciuc MR, Rasanen M, Taavitsainen M, Silvola JM, Saraste A, Hulmi JJ, Anisimov A, Mayranpaa MI, Lindeman JH, Eklund L, Hellberg S, Hlushchuk R, Zhuang ZW, Simons M, Djonov V, Knuuti J, Mervaala E, Alitalo K. VEGF-B-induced vascular growth leads to metabolic reprogramming and ischemia resistance in the heart. *EMBO Mol Med* 2014;**6**:307–321.

37. Bougioukas I, Didilis V, Ypsilantis P, Giatromanolaki A, Sivridis E, Lialiaris T, Mikroulis D, Simopoulos C, Bougioukas G. Intramyocardial injection of low-dose basic fibroblast growth factor or vascular endothelial growth factor induces angiogenesis in the infarcted rabbit myocardium. *Cardiovasc Pathol* 2007;**16**:63–68.

38. Pettersson A, Nagy JA, Brown LF, Sundberg C, Morgan E, Jungles S, Carter R, Krieger JE, Manseau EJ, Harvey VS, Eckelhoefer IA, Feng D, Dvorak AM, Mulligan RC, Dvorak HF. Heterogeneity of the angiogenic response induced in different normal adult tissues by vascular permeability factor/vascular endothelial growth factor. *Lab Invest* 2000;**80**:99–115.

39. Pontes-Quero S, Fernandez-Chacon M, Luo W, Lunella FF, Casquero-Garcia V, Garcia-Gonzalez I, Hermoso A, Rocha SF, Bansal M, Benedito R. High mitogenic stimulation arrests angiogenesis. *Nat Commun* 2019;**10**:2016.

40. Bussani R, De-Giorgio F, Abbate A, Silvestri F. Cardiac metastases. *J Clin Pathol* 2007;**60**:27–34.

## Translational perspective

Cardiac ischaemia is a leading cause of morbidity and mortality worldwide. Various clinical trials have attempted to revascularize ischaemic hearts through the delivery of pro-angiogenic molecules, but they have invariably failed. Our results indicate that cardiac endothelial cells sense pro-angiogenic stimuli but are not able to drive an efficient angiogenic response. This poor angiogenic potential is also associated with reduced growth of cancer cells in the heart. This work provides some mechanisms behind the poor angiogenic capacity of the heart and paves the way to future strategies for the therapy of both cancer and cardiac ischaemia.